# A CMOS Electrochemical Impedance Spectroscopy (EIS) Biosensor Array

Arun Manickam, Aaron Chevalier, Mark McDermott, Andrew D. Ellington, and Arjang Hassibi

***Abstract*—In this paper, we present a fully integrated biosensor $10 \times 10$ array in a standard complementary metal–oxide semiconducor process, which takes advantage of electrochemical impedance spectroscopy (EIS). We also show that this system is able to detect various biological analytes, such as DNA and proteins, in real time and without the need for molecular labels. In each pixel of this array, we implement a biocompatible Au electrode transducer and embedded sensor circuitry which takes advantage of the coherent detector to measure the impedance of the associated electrode-electrolyte interface. This chip is capable of concurrently measuring admittance values as small as $10^{-8}\Omega^{-1}$ within the array with the detection dynamic range of more than 90 dB in the frequency range of 10 Hz-50 MHz.**

***Index Terms*—Biosensor, DNA, electrochemical analysis, electrode, impedance spectroscopy, microarray, proteins.**

## I. Introduction

BIOSENSORS are devices that use biological elements to identify and detect various molecules and biochemical analytes [1]. The detection methodology of a biosensor is based on coupling a biological recognition and capturing element (i.e., capturing a probe molecule), with a transducer and create a measurable signal (e.g., optical or electrical) when analytes are captured. The selectivity of the molecular-level capturing determines the specificity and ultimately the signal-to-noise ratio (SNR) of the sensing. Biosensors are known to be versatile and are implemented in numerous applications, ranging from environmental testing and monitoring [2] to molecular diagnostics [3]. In addition, they can easily be placed in an array (DNA and protein microarrays [4], [5]) to simultaneously identify and measure the concentration of thousands of analytes in the sample.

Although biosensing has a simple concept (i.e., capture and "count"), the output signals of biosensors typically have low SNRs [6]. This is due to the fact that the biosensing process is susceptible to a significant amount of biochemically- and biologically-originated errors which generally overwhelm the signal and limit the detection dynamic range (DDR). Today, there are different approaches which can enhance the DDR of biosensors. To reduce the effects of interference, for example, reporter or label molecules (e.g., fluorescent tags [4] or nanoscale particles [7]) are used. An alternative approach is to use assays and transducers that enable real-time measurements and take advantage of the kinetics-based estimation that is less vulnerable to background signals [8], [9]. While these approaches significantly improve the DDR, they are not "free" and generally necessitate complicated and bulky instrumentation. This, in turn, limits the use of most biosensors in point-of-care (PoC) bioanalysis applications where portability and ease of use is critical.

Research trend has emerged recently which has the potential to address certain challenges of biosensors and deliver systems which not only have high DDR, but also serve as integrated solutions. The general idea is to use standard CMOS integrated circuits (ICs) as the "backbone" for the biosensor platform. The reported transduction modalities of these systems have been diverse and demonstarted the fact that CMOS can accommodate visible-range optical [10], electroanalytical [11]–[14], and magnetic [15] biosensors. R. Brown *et al.* provides a good review on some of the existing integrated chemical sensor platforms [16]. It is imperative to understand that the driver behind using conventional CMOS, as opposed to custom fabrication processes, is the superior electronic sensing capabilities of CMOS, while offering a high level of integration, cost efficiency, and large-scale manufacturing.

The goal of this paper is to demonstrate, for the first time, the design and implementation of a fully integrated impedance-based CMOS biosensor system. The transduction modality used in this system [i.e., electrochemical impedance spectroscopy (EIS)], is widely used in electroanalysis and biosensing [17], [18]. In EIS, the small impedance changes that occur in an electrode-electrolyte interface that are generated by molecular capturing are detected in real time and then are correlated to the presence of target analytes. The main advantages of EIS are its label-free and real-time detection capabilities. Furthermore, EIS is a noninvasive electroanalytical measurement technique when compared to techniques such as cyclic voltammetry (CV) as the potentials applied to the surfaces are very small (typically 10–20 mV amplitude sinousoids). It provides a lot more information when compared to capacitance or conductivity based measurement techniques. The main drawbacks of EIS however are its low transduction gain (i.e., very small impedance changes due to capturing), and the inherent complexity of its instrumentation. Our challenge in this research has been to leverage the capabilities of IC technology to not only design high dynamic range impedance detectors for biosensing, but also integrate an array of them in a single CMOS chip to enable multiplexing. The chip has an array of on-chip electrodes which serve as electrochemical transducers. Electrode arrays have been routinely used in biomedical applications such as neural signal recording, cellular signal monitoring and cell based assays [19]–[23]. They are

Manuscript received June 16, 2010; revised September 06, 2010; accepted September 21, 2010. Date of publication November 11, 2010; date of current version November 24, 2010. This paper was recommended by Associate Editor H.-J. Yoo.

The authors are with the University of Texas at Austin, Austin, TX 78712 USA (e-mail: mmarun@ mail.utexas.edu; arjang@mail.utexas.edu).

Digital Object Identifier 10.1109/TBCAS.2010.2081669

used for applying electrical stimuli to the cells and for recording action potentials. On-chip electrode arrays with $128 \times 128$ electrodes have been demonstrated [20]. In our work, we designed the system to be an open-platform by making its electrode transducers compatible with conventional EIS assays.

Initially in Section II of this paper, we introduce the system-level issues of EIS biosensors, the electroanalytical transducer design, and the proposed impedance detection methodology. In Section III, we discuss the IC implantation using a standard CMOS process, followed by both the electrical and biological experimental results in Section IV.

## II. EIS Biosensor System

We have two main objectives in the design of the EIS biosensor chip. The first is to leverage the capabilities of standard CMOS processes to create a fully electronic biosensor system which includes not only the electroanalytical transducers, but also the detection and interface circuits. The second is to ensure its compatibility with the state-of-the-art electroanalytical assays, reagents, biotechnology applications, and capturing probe immobilization methods. The former objective, if delivered, guarantees cost-efficiency, large-scale manufacturability and compactness, while the latter makes it a viable open-platform system in biotechnology. On top of these, we designed the transducers and circuits to offer real-time detection capabilities while maximizing the impedance DDR. In Sections II-A–C, we explain these in great detail.

### A. EIS Electrode Design

The sensing electrodes in EIS may use a variety of capturing molecules for detection. These molecules come in with different sizes, molecular weights, and charge densities. For example, a short 30 base pair (bp) oligonucleotide in DNA-based biosensors can weigh about 9.9 kDa, while an immunoglobin A (IgA) antibody used in EIS immunoassays weights more than 70 kDa. [25]. These molecules can also exhibit different levels of hydrophobicity and hydrophilicity and hence interact differently with the molecules on the electrode surface. As a result, it is critical that one takes all of the physiochemical characteristics of the probes into consideration when designing EIS systems. Additionally, it is critical to select a proper material for the conducting electrode and linker molecule between solid electrode surface and the capturing probe.

It is important to realize that EIS methods are not limited to bio-molecular detection and they also have been used in cell-based assays [19], [24] in order to perform real-time studies of cell growth and death under different ambient conditions. The only difference is that the electrode fabrication in these applications requires a large number of post-CMOS steps which increase the cost and complexity of manufacturing.

To demonstrate the feasibility of creating an open-platform biosensor array using standard CMOS processes, we decided to target the most widely used electrode which is gold (Au) [26]–[28]. The main reason for popularity of gold in electroanalysis (and EIS) is that it is not only inert (i.e., does not corrode with nonzero biases on the interface), but also biocompatible. For example, one can take advantage of different thiol-based immobilization chemistries to cross-link capturing molecules to it [27], [28].

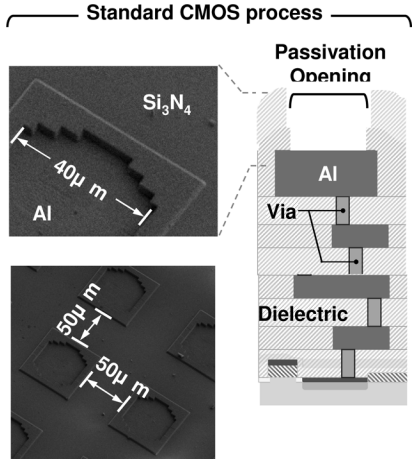


Fig. 1. Passivation openings in standard CMOS structure used as sensing electrodes. The dimensions of the electrode and the spacing between them are shown in the SEM pictures.

The electrodes in our array are created by first forming passivation openings on the top metal layer of the CMOS process, as it is done for I/O pads as illustrated in Fig. 1. The exposed metal surfaces are approximately 40 $\mu$m$\times$ 40 $\mu$m and are separated by 50 $\mu$m (see Fig. 2). The top metal layer in a standard CMOS process is predominantly made of aluminum (Al) with certain impurities [29]. Using the Al surface as an EIS electrode has an inherent disadvantage since Al is not chemically inert and quickly forms an oxide layer on exposure to air. Unlike gold (Au) or platinum (Pt), Al also corrodes easily if the applied bias is greater than 300 mV [30]. To create a universal Au electrode surface, we used an electroless nickel (Ni) immersion Au (ENIG) plating process [31] to first form Ni and then Au on the exposed Al surface (see Fig. 2). The rationale behind changing the surface to Ni first is that Au cannot be plated on Al surfaces directly and an intermediate layer is necessary. This method does not require the use of masks since Ni and Au layer cannot be formed on the passivation layer. The thicknesses of the Ni and Au layers are selected to be 2 $\mu$m and 200 nm, respectively. At this point, the Au surface can be biofunctionalized using thiol-based protocols where the sulfur in the thiol group can form a covalent bond to the Au surface and act as the anchor for the different linker molecules. As shown in examples of Fig. 3, in the case of DNA-base biosensors, the single-stranded DNA (ssDNA) are thiol modified on one end to directly attach to the Au electrode [27], where for protein detection assays, an indirect attachment technique can be adopted using linker molecules such as 11-Mercaptoundecanoic acid (11-MUA). As illustrated, such molecules attach from one side to the capturing protein (e.g., antibody) and from the other side to the Au surface [32].

### B. Impedance Detection

The goal of the detection circuitry in EIS systems is to measure, in real time, the admittance of the electrode-electrolyte interface, denoted by $Y(\omega)$. In an array format, we need to measure $Y(\omega)$'s of all pixels in parallel and independently. To do

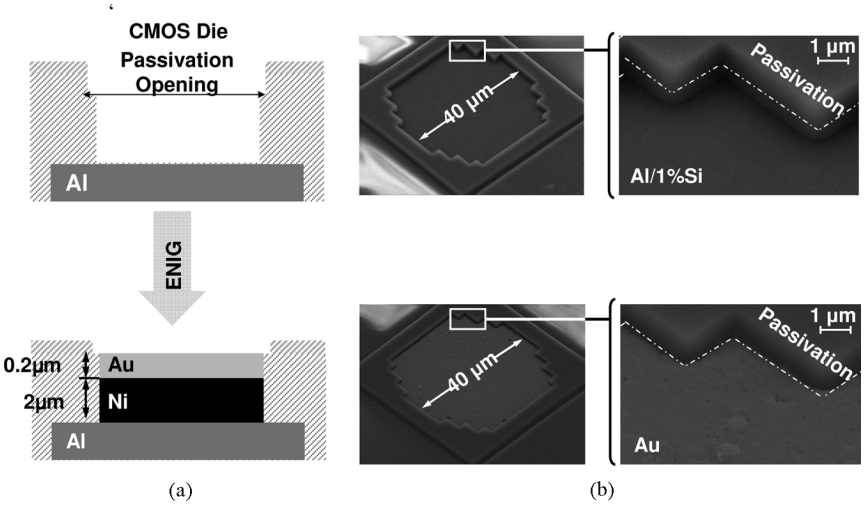


(a) (b)

Fig. 2. (a) Top layers of a CMOS process, where using an electroless nickel immersion gold (ENIG) process [23] we create Au sensing electrodes, and (b) SEM picture of surface before and after the ENIG process.

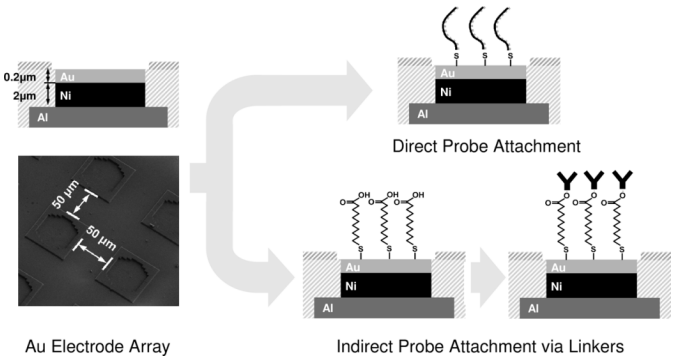


Fig. 3. Capturing probe immobilization example methods for the Au sensing electrodes.

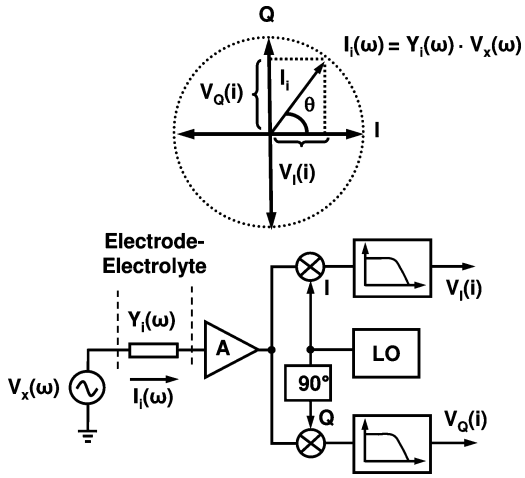


Fig. 4. Coherent detection architecture for the impedance measurement.

this in our biosensor system, we place a large and shared reference electrode in the solution which is a highly conductive electrolyte to establish the sinusoidal excitation voltage signal $V_x(\omega)$ across all electrodes. Next, we measure the flowing current through each electrode, $I(\omega)$ and compute the electrode-electrolyte admittance of the $i$th pixel, $Y_i(\omega)$, using the following formula:

$$\frac{Y_i(\omega) = I_i(\omega)}{V_x(\omega)} \tag{1}$$

where $I_i(\omega)$ is the measured current at the $i$th pixel. Since all signals in this EIS are sinusoidal, to find $Y_i(\omega)$, we only need to calculate the relative amplitude and phase shift of $I_i(\omega)$ compared to $V_x(\omega)$. To carry this out, we take advantage of coherent detection techniques (also called direct conversion architecture) to obtain the phase and amplitude information of $I_i(\omega)$. As shown in Fig. 4, we first amplify the current $I_i(\omega)$ in each pixel by means of a low-noise transimpedance amplifier (TIA) with a gain of $A$. The output of TIA is then multiplied by orthogonal sinusoidal signals (I and Q) at frequency $\omega$. Subsequently, we take advantage of a low-pass filter to remove the higher-order harmonics that are generated by the mixing operation. The dc value at output of I and Q channels of the $i$ th pixel, denoted by $V_I(i)$ and $V_Q(i)$, respectively, are can be then used to estimate the amplitude and phase of $Y_i(\omega)$ using

$$|Y_i(\omega)| = \frac{\sqrt{V_I^2(i) + V_Q^2(i)}}{A \cdot |V_x(\omega)|} \tag{2}$$

and

$$\angle Y_i(\omega) = \tan^{-1}\left(\frac{V_Q(i)}{V_I(i)}\right). \tag{3}$$

### C. System Architecture

The overall chip architecture is shown in Fig. 5. The system consists of an array of $10 \times 10$ pixels where the column and row decoders are used to scan the array and access the individual outputs of pixels. This approach is similar to the readout structure of CMOS image sensors [33]. Each pixel within the array consists of one sensing electrode and one coherent detector which include the low-noise TIA for current amplification and two mixers (I and Q) for signal multiplication. The role of

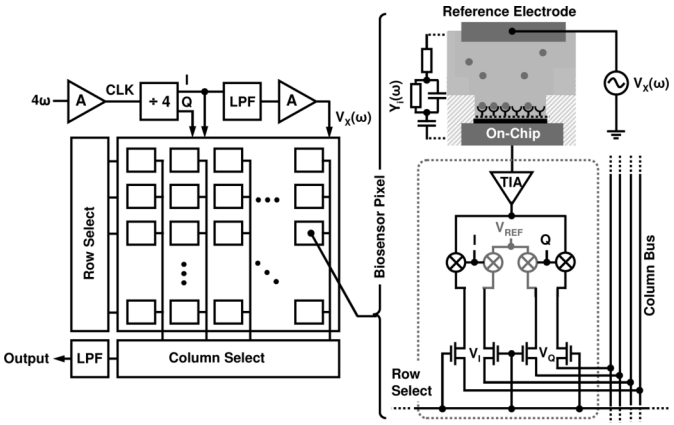


Fig. 5. System architecture.

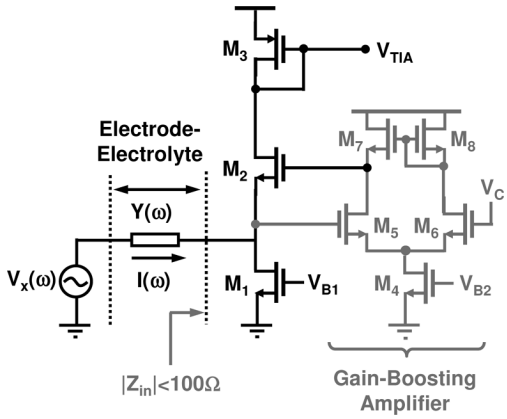


Fig. 6. Circuit diagram of the transimpedance amplifier (TIA).

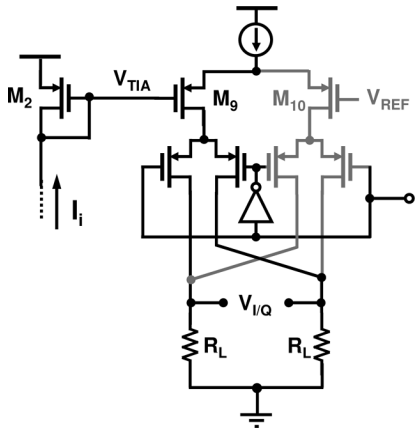


Fig. 7. Circuit diagram of the mixer.

$V_{\rm REF}$ of Fig. 5 is explained in subsequent sections. The reference electrode, which establishes $V_x(\omega)$ within the electrolyte, is an external component (i.e., not integrated), and is immersed into the electrolyte solution. The capturing probe of each pixel can be different and, hence, this particular system can be used to detect up to 100 different analytes when utilizing all pixels for biosensing.

The quadrature I and Q signals as well as $V_x(\omega)$ are generated within the system using an external reference clock operating at $4\omega$. We did not integrate the clock generator to maximize testability, tenability, and ease of characterization. The $4\omega$ clock first goes through a divide-by-4 digital counter to generate the necessary quadrature (90° phase shifted) I and Q square-wave signals at $\omega$. The excitation signal $V_x(\omega)$ is derived from the I signal (using a low-pass filter and an amplifier) and, therefore, is phase-locked to it. The main advantage of this approach is that by sweeping the $4\omega$ clock, we can sweep $\omega$ and measure $Y(\omega)$ without modifying the readout circuit which operates independent of $\omega$ at low frequency. Yet, we still need to guarantee that the TIA and mixers function properly in the desired frequency range. We will discuss this in detail in Section III.

## III. IC Implementation

### A. Transimpedance Amplifier (TIA)

The main objective of the low-noise TIA, beside amplification, is to keep a low impedance node at the sensing electrode contact. This is to ensure that $Y(\omega)$ remains proportional to $I(\omega)$ only, and not a function of the TIA input impedance. As illustrated in Fig. 6, we have selected a common-gate topology for the TIA using transistors M1-M3. To decrease the input impedance of the TIA, we also gain-boost M2 by using a differential amplifier made of transistors M4-M8. If we consider the gain of this differential amplifier to be $A_d = g_{m5}(r_{05}||r_{07})$, then $Z_{\rm in}$, the input impedance of the gain-booted TIA becomes

$$Z_{in} \approx \frac{1}{g_{m2}A_d} = \frac{1}{g_{m2}g_{m5}(r_{05}||r_{07})}. \quad (4)$$

The TIA of this system is designed so the value of $|Z_{\rm in}|$ always remains below 100 Ω for frequencies up to 50 MHz. These criteria guarantees that for a typical electrode-electrolyte interfaces impedance (e.g., $|Y(\omega)| \geq 10$ kΩ), the error always remains below 1%. The TIA gain, $A_{\rm TIA}$, in this particular topology is equal to $g_{m3}^{-1} \approx 13\,\text{k}\Omega$, which is the input impedance of the diode connected M3.

The role of the differential amplifier is to not only reduce $|Z_{in}|$, but also set the dc potential of the sensing electrode. This dc potential is set by applying of an external voltage, $V_c$, to the positive input of the differential amplifier. The error voltage is a function of the loop gain and approximately equal to 0.005 for $A_d = 45$ dB which is the nominal dc gain of the differential amplifier. This feature is particularly beneficial in controlling Faradaic processes (i.e., oxidation and reduction) that may occur due to the potential difference between the solution and the sensing electrodes. The value of $V_c$ in our system can vary between 0.9 V to 2 V without affecting the functionality of the TIA, making it possible to measure admittance while applying dc voltage stimulations on the sensing electrode.

One key consideration in the design of TIA is its noise performance. The leading noise contributors are the current source M1 and the load transistor M3. In the common-gate structure M2 acts as a cascade transistor and hence has little effect on the noise performance. The noise from the differential amplifier is also negligible here. This is because its output voltage noise has a small gain (i.e., $g_{m2}(1+g_{m2}r_{01})^{-1}$), when referred to the TIA input current. As a result, the input-referred current noise power

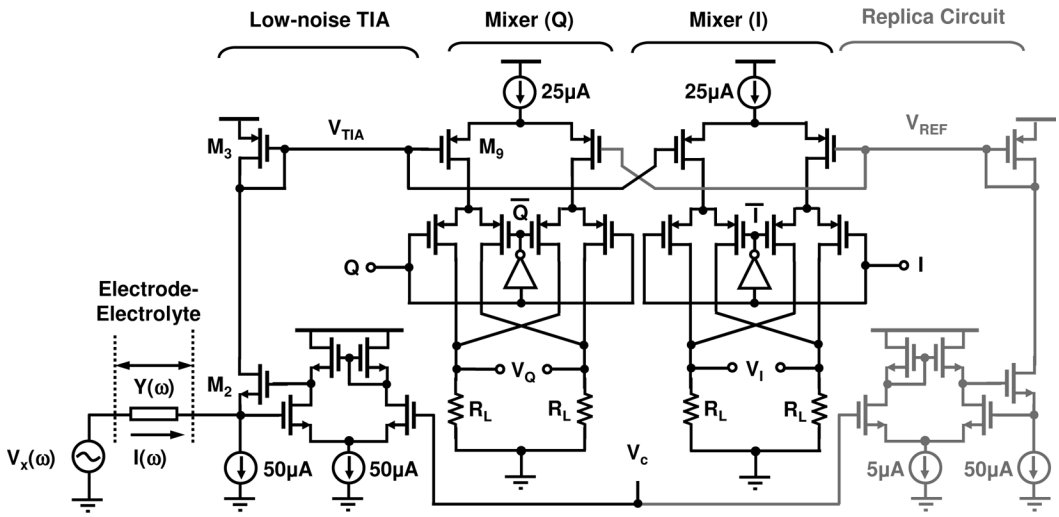


Fig. 8. Circuit diagram of the entire pixel (excluding bias circuits).

spectral density (PSD) of the TIA, denoted by $\overline{I^2_{n-ref}(\omega)}$, can be formulated by

$$\overline{I^2_{n-ref}(\omega)} \approx 4kT(\gamma_1 g_{d01} + \gamma_3 g_{d03}) \tag{5}$$

where $g_{d0}$ is the zero-bias drain source transconductance, and $\gamma$ is a bias dependant noise coefficient of the associated transistors.

In (5), one should also include the 1/f noise contributions of M1 and M3; yet we neglected these fluctuations and only included their thermal noise component. This is due to the fact that we have a narrow\band coherent "receiver" architecture in the signal chain. In these architectures, similar to most RF receivers, and as long as $\omega$ remains above the 1/f noise corner frequency, the 1/f noise becomes "out-of-band" and, thus, need not be present at the output of the low-pass filter. The 1/f noise corner frequency in our system is designed to be 100 kHz, which is achieved mainly by increasing the lengths of M1 and M3 to 5 $\mu$m and 1 $\mu$m, respectively.

The current through the common gate stage in this design is 50 $\mu$A. Although this current can be lowered without significantly loosing the gain and noise performance of the TIA, we intentionally kept it high to measure $|I(\omega)|$'s in the order of 10–20 $\mu$A with sufficient linearity. The differential amplifier bias current is also set to 50 $\mu$A, but this is to achieve a sufficient gain-bandwidth requirement (i.e., minimum gain of 30 dB at 50 MHz), and ensure $|Z_{in}| < 100\ \Omega$.

### B. Quadrature Mixers

To multiply $I(\omega)$ by the I and Q quadrature signals, as shown in Fig. 7, we connect the diode-connected output of the TIA, $V_{\rm TIA}$, to the input of two double-balanced differential Gilbert cell mixers. For the sake of clarity, only one of the two identical mixers is shown. Differential Gilbert cell mixers [34] are widely used as they greatly reduce the LO leakage to the outputs and relax the filtering requirements at the output. Also, having differential outputs is beneficial for sensor arrays as they are less prone to interference, IR drops, and other nonidealities. In the mixers, the transconductance of M9-M10, denoted by $g_{m9}$, in the input differential pair is set to be equal to $g_{m3}$. To minimize the 1/f noise contributions of the mixers, we also use resistors $(R_L = 50\ \mathrm{k}\Omega)$ instead of implementing active transisitor loads. Based on this type of configuration, the total transimpedance gain of the system $A_{Total}$ becomes

$$A_{Total} \approx A_{\rm TIA} \cdot (-g_{m9} R_L) = -R_L. \tag{6}$$

Now since the output of the TIA (positive input of the differential mixer) is single ended, we have to generate a stable dc reference voltage $V_{\rm REF}$ for the other input (negative input of the differential mixer). As shown in Fig. 8, this is done placing a replica circuit with an identical structure as the low-noise TIA. There is only one difference between the TIA structure and the replica circuit. In the replica circuit, the bias used for the differential amplifier is only 5 $\mu$A instead of 50 $\mu$A since it only needs to operate at dc and, hence, has a relaxed gain-bandwidth requirement. The overall current consumption of the pixel is 220 $\mu$A (including the bias circuits in each pixel) with a 3.3-V supply with a total area of 100 $\times$ 100 $\mu$m.

It is important to realize that the large size of the biosensor array makes the pixel-to-pixel gain and dc offset variations inevitable. This phenomenon is somewhat comparable to the fixed pattern noise (FPN) in CMOS image sensor arrays [33]. In our case, offset and gain variations are primarily caused by the mismatch between the load resistors of the mixers. Gain variation in this system is measured to be around $\pm$0.6 dB over the entire array. Accordingly, one needs to pay careful attention to the layout and physical dimensions of these devices to ensure acceptable nonidealities.

### C. I and Q Generation

The chip has a built-in divide-by-4 generator which accepts the $4\omega$ reference clock and generates the necessary I and Q signals that are required for the operation of the mixers. As illustrated in Fig. 9, we use a self-biased inverter to recover the ac-coupled clock signal. The self-biased inverter reduces the sensitivity of the circuit to the amplitude and dc bias point of the input sinusoid. It also sets the dc bias point at the threshold voltage of the inverter (approximately to 1.65 V in our design)

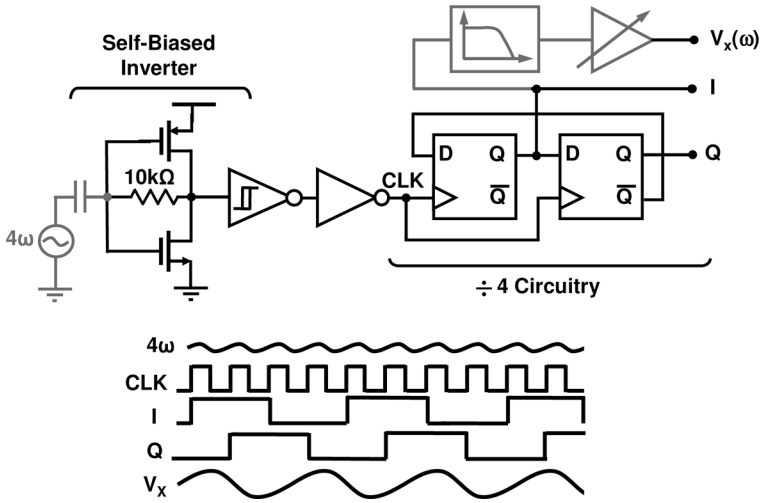


Fig. 9. I/Q generator (the gray blocks are off-chip components).

with a small-signal gain of 3.5. The main disadvantage of self-biased inverters is their sensitivity to glitches in the power supply. In order to eliminate this impediment, a Schmitt trigger buffer [35] is used after the self-bias inverter. This buffer creates a voltage window of approximately 1 V around the transition region, making gate insensitive to any glitch within this window. The output of Schmitt trigger is then buffered and applied as the clock input (CLK) of two flip flops that serve as the divide-by-4 circuitry. The rationale behind using this topology is that we can reliably generate accurate I and Q for a wide range of frequencies. Our measurements demonstrated that the achieved phase error is less than 0.2 degrees over the 10 Hz to 50 MHz frequency range. The I signal is subsequently taken off chip, low pass filtered, and passed through a variable gain amplifier to create $V_x(\omega)$. The typical amplitude for $V_x(\omega)$ in this system is between 10–20 mV. It is essential to make sure that there is a fixed phase offset between $V_x(\omega)$ and I signals as any drift in phase during the measurement could lead to inaccurate phase as well as magnitude measurements. The fixed phase offset can be calibrated using standard resistors with the entire setup in place.

In Fig. 10, we show the chip micrograph of the biosensor IC which was designed and fabricated using a 0.35 $\mu$m bulk CMOS process. The total chip size is 2 mm $\times$ 2 mm, with the biosensor $10 \times 10$ array occupying 1 mm $\times$ 1 of this area.

## IV. Results and Discussion

The IC measurement setup is shown in Fig. 11. The inputs to the EIS biosensor chip are the external reference clock operating at $4\omega$ (from Agilent 33120A) and the digital inputs to the decoder (from NI PCI 6289). There are two differential outputs in this system (i.e., $V_I$ and $V_Q$), which are first multiplexed, amplified and filtered using a low noise preamplifier (SRS560). and later digitized using the NI PCI 6289 acquisition system. The whole setup is computer controlled by means of a GPIB port, which also synchronizes the excitation and data collection signals of the test system.

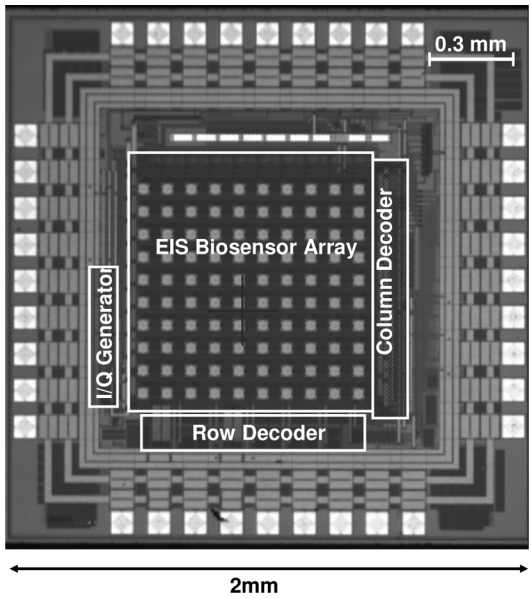


Fig. 10. Die photograph.

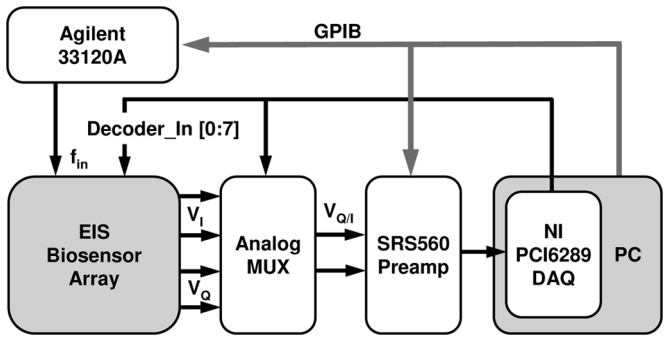


Fig. 11. Measurement setup.

Before calculating the admittance using (2) and (3), we subtract the dc offset of each pixel which is measured prior to experiments and under input open-circuit conditions (i.e., no solution present). Using this setup and dc offset calibration procedure,

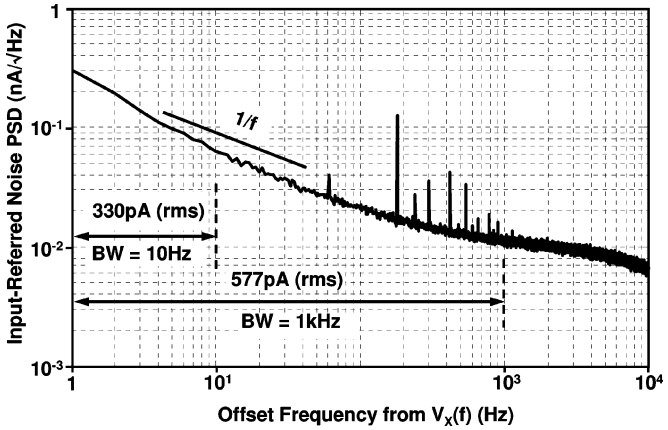


Fig. 12. Pixel-level input-referred noise power spectral density (PSD).

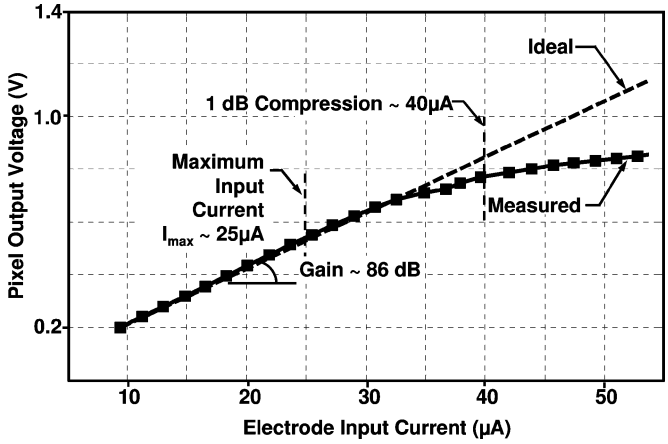


Fig. 13. Linearity performance of the pixel.

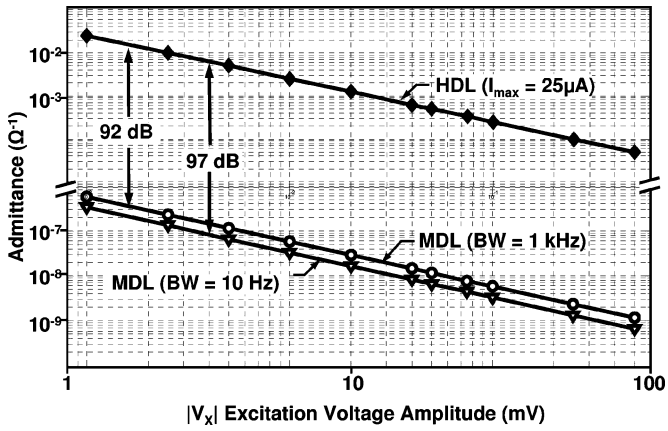


Fig. 14. Admittance measurement limits.

we are able to perform automated admittance measurements accurately at a large number of frequency points over the entire array.

### A. Admittance Detection Limits

In order to calculate the impedance sensitivity (i.e., minimum detection level) of the system, we need to consider its noise performance of the pixels. The noise from of the signal path at the output, prior to low-pass filtering, is measured under input open-circuit conditions with an excitation frequency of 2.5 MHz. Fig. 12 shows the input-referred current noise PSD, which is essentially the output noise divided by $A_{\mathrm{Total}}$.

Now, to evaluate the current sensitivity of this system, we need to integrate the current noise PSD over a specific bandwidth to find its rms value. As one can see in Fig. 12, this value is 330 pA rms and 577 pA rms for 10-Hz and 1-kHz bandwidths, respectively. While lowering the cutoff frequency of the low-pass filter, $f_c$ results in better noise performance, it reduces the overall measurement speed, and the array scan rate. Considering that the required settling time for 16-bit accuracy is approximately $11 f_c^{-1}$, we need about 110 s to perform one full scan of all the 100 pixels for $f_c = 10$ Hz, while for the case of $f_c = 1$ kHz, this value is 1.1 s. This level of sensitivity is sufficient for most EIS applications since further improvement is limited by the thermal noise contribution of the electrolyte resistance [36]. In this topology, since we use resistors as the load of the mixers and relatively large devices (with widths $> 1\,\mathrm{um}$), the flicker noise contribution becomes less problematic for excitation frequencies larger than 50 kHz.

The upper limit of impedance detection is set by the linearity of the signal chain. The linearity is measured here by placing a 10-k$\Omega$ resistor at the input of the TIA while we vary the amplitude of $V_x(\omega)$. The output amplitude $|V_0|$ is then calculated by using the measured values of $V_I$ and $V_Q$ based on

$$|V_0| = \sqrt{V_I^2 + V_Q^2}. \tag{7}$$

In Fig. 13, we show the measured $|V_0|$ as a function of $|V_x(\omega)|$. For currents smaller than 20 $\mu$A, the response is linear with a constant slope equal to $|A_{Total}| = 86$ dBV/A. As the current increases, the circuit enters a nonlinear region where the 1-dB compression point is approximately 40 $\mu$A. One inherent disadvantage of using coherent receivers is that the dc output generated by the second order nonlinearities directly affects the measured $V_I$ and $V_Q$ at dc. Accordingly, we chose the safe upper limit of detection $I_{\max}$ to be 25 $\mu$A, which is based on backing off sufficiently from the 1-dB compression point.

Now, we can calculate the admittance minimum detection level (MDL) and highest detection level (HDL) using the measured noise rms value which sets the MDL and $I_{\max}$ value which sets the HDL. As plotted in Fig. 14, for $|V_x(\omega)| = 10\,\mathrm{mV}$, this system is capable of measuring $\Delta|Y(\omega)|$ of 10 nS for $|Y(\omega)|$ as high as 1 mS. This is approximately 97-dB DDR which is maintained over a wide range of excitation frequencies from 10 Hz to 50 MHz. To the best of our knowledge, this is the highest reported DDR ever for an admittance measurement system. The overall chip performance and its key metrics are listed in Table I.

### B. Electrochemical Measurements

For performing EIS experiments, we need to bring the sensing electrode array in contact with the solution (electrolyte). To do this without interfering with the electronic data acquisition, we isolate the conductive solution from the bond-wires, I/O pads, and the IC package by using an electrically insulating epoxy

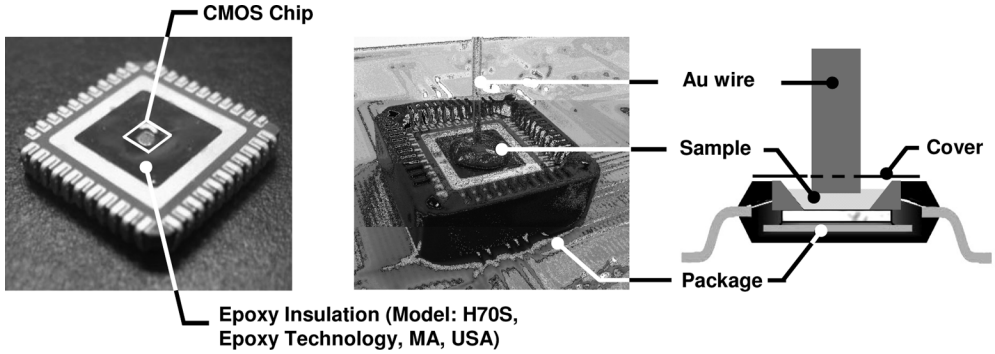


Fig. 15. Packaging and electrochemical experimental setup.

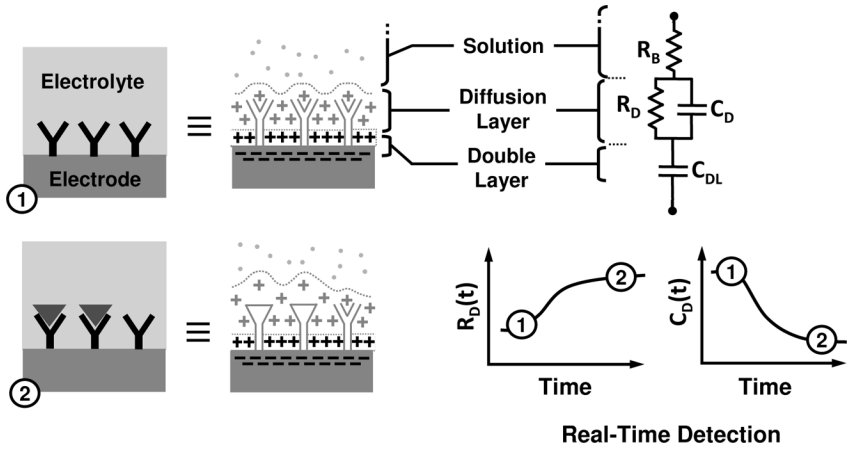


Fig. 16. Detection principle of the EIS system. Top half figure shows the charge profile close to the interface and equivalent circuit parameters of an electrode-electrolyte system. The bottom half shows the changes in impedance of the diffusion layer that occurs with probe-analyte binding, which permits the detection of the analyte.

TABLE I
MEASURED PERFORMANCES OF THE EIS BIOCHIP

| | |
|---|---|
| Technology | 0.35μm CMOS, 4 metal layers, 3.3V supply |
| Die Size | 2mm × 2mm |
| Array Size | 10×10,100μm×100μm |
| Electrode | 40μm×40μm, Al/1% Si |
| Frequency range | 10Hz – 50MHz |
| Power consumption | 84.8mW (100KHz) |
| Current sensitivity(BW=10Hz) | 330pA |
| 1 dB compression point | 40μA |
| Dynamic Range(BW = 10Hz) | 97dB |
| Scan rate (BW=10Hz) | 0.55 $min^{-1}$ |

(EPOTEK H70S), as shown in Fig. 15. Subsequently, the reference 1-mm diameter Au wire electrode is immersed into the solution carefully on top of the sensing surface.

To correlate the EIS measurements with the physiochemical aspects of the system, it is essential to understand the equivalent compact circuit model of an electrode-electrolyte interface. The basic compact impedance model for an electrode-electrolyte system [17], [37] is shown in Fig. 16. The charge profile close to the interface is shown. Close to the interface, we have a fixed layer of oppositely charged ions, which constitute the double layer [17]. $C_{\rm DL}$ is the capacitance of the double layer. Further away from the interface, we have the diffusion layer, which is where the capturing probe molecules are located. Its impedance is represented by a combination of $R_D$ and $C_D$. Finally, $R_B$ represents the bulk resistance of the electrolyte. Generally speaking, the bulk resistance of the electrolyte is dominated by the properties of ions in the solution as number of analyte molecules is much lesser than number of ions in the solution. Now, as the analytes get captured at the surface, the overall charge distribution and the mobility of the ions at the diffusion layer change. This, in turn, alters $R_D$ and $C_D$ [17], which can be detected in real time by monitoring the impedance.

Each additional layer of molecules can be modeled by a parallel RC element in series with the other layers. Hence, by properly choosing equivalent circuit model, EIS can be used to study into various distances from the electrode-electrolyte interface.

Many models for electrode-electrolyte systems include a charge transfer resistor $R_{CT}$, which appears in parallel with the double layer capacitance $C_{DL}$. In our case, it is possible to neglect the contribution of this resistor since thiolated probe molecules form a densely packed monolayer on gold surface. These densely packed layers almost completely block charge transfer and in most cases can be modeled as an ideal capacitor with negligible leakage [38].

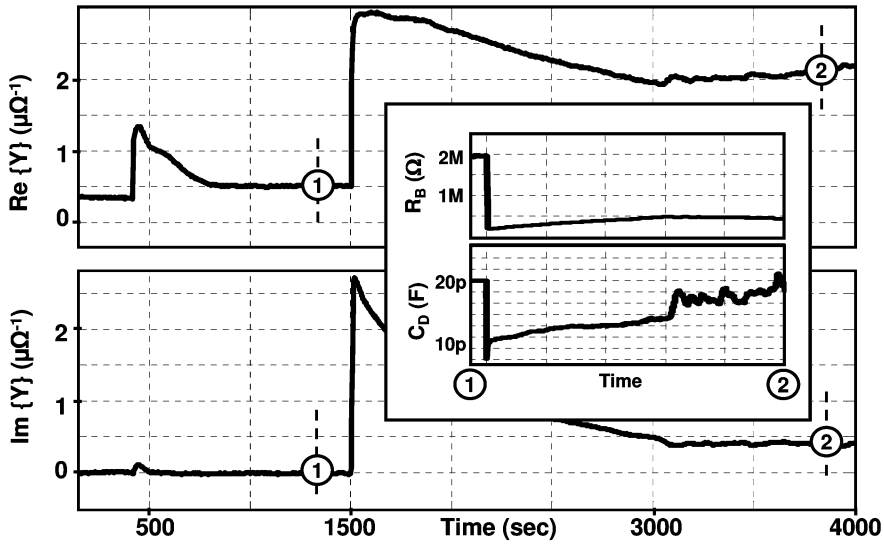


Fig. 17. Real-time control experiments performed with KCl buffers. Initially, 120 $\mu$l of 1-mM KCl is present into which 6 $\mu$l of 10 mM and then 6 $\mu$l of 100-mM KCl are added at 450 s (1) and 1500 s (2) from the start of the experiment. The curves inset show the changes in the bulk resistance and interfacial capacitance with the addition of 6 $\mu$l of 100-mM KCl.

In the waveforms of Fig. 17, we show a real-time impedance measurement example which is performed in KCl buffer. In this setup, the salt concentration is changed twice during the experiment. Initially 120 $\mu$l of 1 mM KCl is present into which 6 $\mu$l of 10 mM and then 6 $\mu$l of 100 mM KCl are added. The measurements results are done at $\Omega = 100$ kHz and data points are collected with a rate of $10^3\ sample \cdot \sec^{-1}$. By carefully studying these results, we can identify the exponential settling of the admittance values which indicate the relaxation of the interface charge distribution. In this example, $R_B$, decreases as we increase the ionic strength (salt concentration) of the solution. Yet, the surface capacitance increases. This is due to the fact that there is closer ionic shielding near the interface when the ionic strength is larger [37]. It is important to recognize that real-time detection capability in the EIS biosensor system is significant since few commercially available biosensor platforms offer this feature. Moreover, we believe this feature to be instrumental in understanding reaction mechanisms in biosensors while arriving at better estimates for analyte concentrations.

Though real-time detection enable kinetic analysis, conventional EIS methods still need to evaluate equilibrium values of admittance. To demonstrate this feature in our chip,, we measured the admittance spectra of some of the common buffers used in biology first. The admittance spectra are measured with zero dc potential difference between the reference electrode and the sensing electrode. In the Nyquist plots shown in Fig. 18, the imaginary part of $Y(\Omega)$ is plotted vs. the real part. As one can clearly see, the admittance values of different buffers could vary by five orders of magnitude which are consistent with their computed ionic strength and conductivity. This admittance data is then fitted into equivalent circuit model by making use of a complex nonlinear least square-fitting tool [39]. The equivalent circuit parameters are shown in Table II. This specific set of measurements verifies the DDR of our biosensor system and proves that it can operate in low-conductance as well as high-conductance regimes.

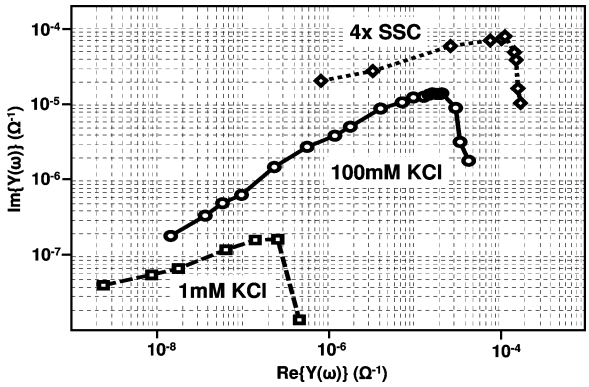


Fig. 18. Admittance spectra of three different biological buffers (1 mM KCl, 100 mM KCl, 4 × SSC) measured under equilibrium condition.

TABLE II
EQUIVALENT CIRCUIT PARAMETERS FOR BIOLOGICAL BUFFERS

| Buffer | $C_{DL}$ | $R_D$ | $C_D$ | $R_B$ |
|---|---|---|---|---|
| 1mM KCl | 17.9pF | $10^{12}\Omega$ | 21.2pF | 3.3MΩ |
| 100mM KCl | 20pF | 270kΩ | 39pF | 36.8kΩ |
| 4×SSC | 903pF | 72kΩ | 514pF | 9.3kΩ |

## C. Biological Measurements

Detecting DNA hybridization is key to all nucleic acid-based biosensors such as gene expression DNA microarrays. One of the advantages of EIS based biosensor is that it permits label-free detection of DNA hybridization. To show this capability here, we immobilized thiolated ssDNA molecules directly onto the Au electrode surface as the capturing probe. The probe

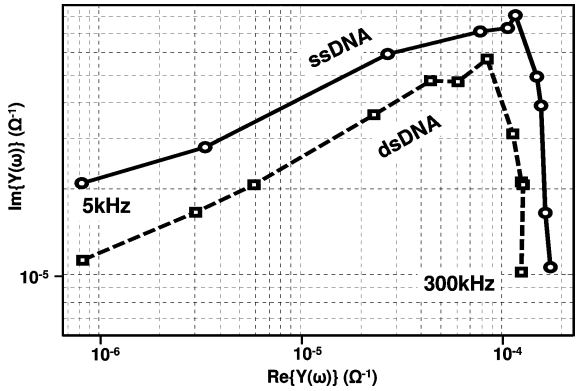


Fig. 19. DNA hybridization experiment. The solid line shows the admittance spectra of ss-DNA and the dotted line shows the admittance spectra of hybridized ds-DNA.

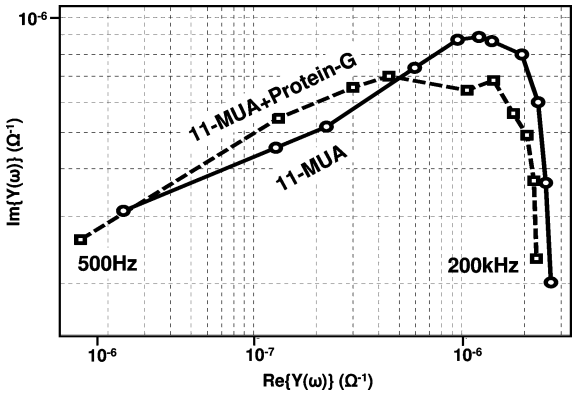


Fig. 20. Protein detection experiment. The solid line shows the admittance spectra of 11 –MUA and the dotted line shows the admittance spectra of 11-MUA with protein-G immobilized onto it.

TABLE III
EQUIVALENT CIRCUIT PARAMETERS FOR DNA HYBRIDIZATION

| | $C_{DL}$ | $R_D$ | $C_D$ | $R_B$ |
|---|---|---|---|---|
| ss-DNA | 300pF | $1.2\times10^{10}\Omega$ | 525pF | 9.36kΩ |
| ds-DNA (Hybridized) | 301pF | $10^{10}\Omega$ | 419pF | 9.36kΩ |

TABLE IV
EQUIVALENT CIRCUIT MODEL FOR PROTEIN DETECTION

| | $C_{DL}$ | $R_D$ | $C_D$ | $R_B$ |
|---|---|---|---|---|
| 11-MUA | 75pF | 149kΩ | 55pF | 422kΩ |
| 11-MUA +protein-G | 162pF | 177kΩ | 76.3pF | 422kΩ |

sequence in this particular experiment is 5'-TGATAGCCCT-GTACAATGCTGCTAAAAAAA-Thiol-3'. The approximate probe concentration is $7\times10^6$ per electrode [40]. The admittance spectrum with immobilized probes is measured in 40 $\mu$l of 4xSSC buffer (solid line in Fig. 19). Onto the same buffer, we add 5 $\mu$l of 1 $\mathrm{ng}/\mu\mathrm{l}$ of complementary ssDNA strand and the admittance spectra of the system is again measured at equilibrium (dashed curve in Fig. 19). This concentration is enough to saturate the whole electrode surfaces. The frequency range is chosen in such a way that the interfacial impedance dominates the response. At higher frequencies, the bulk resistance of the solution dominates the response and the effect of the interfacial impedance cannot be seen. On equivalent circuit fitting (shown in Table III), we observed that while $C_{\mathrm{DL}}$, $R_D$ and $R_B$ remain the same, the value of $C_D$ drops by from 525 pF to 419 pF. This 20% drop in capacitance, has been reported in literature as well [41] and is due to the lowering of dielectric permittivity near the surface. The admittance spectra shown are the average of the response measured at ten different pixel locations in the array. By linear extrapolation of this result and by making use of admittance detection limits derived previously, the limit of detection for our system is around $10^5$ molecules ($6.25\times10^9$ molecules/$\mathrm{cm}^2$). This level of sensitivity makes EIS comparable to other label-free methods of detection that have been reported [12].

Label-free protein detection has always remained a challenge since it is difficult to label protein molecules without generally altering their properties [42]. EIS method is perhaps the ideal candidate as it can perform label-free detection and can probe into varying depths from the electrode surface, providing us with a vast amount of information. In this research, we performed the detection of protein-G molecules which is an immunoglobulin-binding protein that can attach to a wide variety of antibodies. The protocol for immobilization and detection is taken from [43]. A layer of 11-MUA molecules is immobilized on gold surface and the admittance spectrum is measured in 1x PBS buffer. Then, protein-G is immobilized onto the 11-MUA layer and once again the admittance spectrum is measured in 1x PBS buffer. As plotted in Fig. 20, the admittance spectrum exhibits more complex variation when compared with the DNA hybridization experiment. On equivalent circuit fitting (shown in Table IV), we observed changes in $R_D$, $C_D$, as well as $C_{\mathrm{DL}}$. As expected, no change was observed in the bulk resistance. The complicated change in admittance is attributed to the fact that proteins are large molecules with complex charge distribution. This is one of the first ever-reported admittance spectra for on-chip detection of protein attachment. Further studies need to be performed to better understand the changes in the admittance spectra. Nevertheless, EIS provides us with tool for observing the changes that happen near the surface with the attachment of proteins and can be used to perform label-free protein detection.

## V. CONCLUSION

CMOS integrated biosensors are platforms that can leverage very-large scale integration fabrication technologies to provide cost-efficiency, portability, and manufacturability for biosensor platforms. In this paper, we demonstrated that label-free and real-time EIS biosensing can be carried out using CMOS ICs, with only one additional postprocessing step (i.e., gold plating). In this system, we have made use a coherent detector scheme to measure impedance with superior DDR. Our preliminary measurement results indicate that we can perform label-free detection of DNA hybridization and protein attachment, which indicates the versatility of our chip and its potential use in a variety of assays and applications.

## REFERENCES


[1] K. R. Rogers, "Principles of affinity-basedbiosensors," *Molec. Biotechnol.*, vol. 14, no. 2, pp. 109–129, Feb. 2000.

[2] A. J. Baeumner, "Biosensors for environmental pollutants and food contaminants," *Anal. Bioanalyt. Chem.*, vol. 377, no. 3, pp. 434–445, Oct. 2003.

[3] A. D. Weston and L. Hood, "Systems biology, proteomics, and the future of health care: Toward predictive, preventative, and personalized medicine," *J. Proteome. Res.*, vol. 3, pp. 179–196, Mar. 2004.

[4] M. Schena, D. Shalon, R. W. Davis, and P. O. Brown, "Quantitative monitoring of gene expression patterns with a complementary DNA microarray," *Science*, vol. 270, no. 5235, pp. 467–470, Oct. 1995.

[5] G. MacBeath, "Protein microarrays and proteomics," *NatureGenetics*, vol. 32, pp. 526–532, 2002.

[6] A. Hassibi, S. Zahedi, R. Navid, R. W. Dutton, and T. H. Lee, "Biological shot-noise and quantum-limited signal-to-noiseratio in affinity-based biosensors," *J. Appl. Phys.*, vol. 97, no. 8, pp. 084 701–084 701, Apr. 2005.

[7] J. Wang, "Nanomaterial-based electrochemical biosensors," *Analyst*, vol. 130, pp. 421–426, 2005.

[8] J. Homola, "Present and future of surface plasmon resonance biosensors," *J. Analyt. Bioanalyt. Chem.*, vol. 377, no. 3, pp. 528–539, Oct. 2003.

[9] A. Hassibi, H. Vikalo, J. L. Riechmann, and B. Hassibi, "Real-time DNA microarray analysis," *Nucl. Acids Res.*, pp. 1–12, Aug. 2009.

[10] B. Jang, P. Cao, A. Chevalier, A. Ellington, and A. Hassibi, "A CMOS fluorescence-based biosensor microarray," *Proc. ISSCC Dig. Tech. Papers*, pp. 436–437, Feb. 2009.

[11] M. Schienle, C. Paulus, A. Frey, F. Hofmann, B. Holzapfl, P. Schindler-Bauer, and R. Thewes, "A fully electronic DNA sensor with 128 positions and in-pixel A/D conversion," *IEEE J. Solid-State Circuits*, vol. 39, no. 12, pp. 2438–2445, Dec. 2004.

[12] P. M. Levine, P. Gong, R. Levicky, and K. Shepard, "Active CMOS sensor array for electrochemical biomolecular detection," *IEEE J. Solid-State Circuits*, vol. 43, no. 8, pp. 1859–1871, Aug. 2008.

[13] C. S. D. Esposti, C. Guiducci, and C. Paulus, "Fully electronic CMOS DNA detection array based on capacitancemeasurement with on-chip analog-to-digital conversion," *Proc. ISSCC Dig. Tech. Papers*, pp. 48–49, 2006.

[14] F. Heer, M. Keller, G. Yu, J. Janata, M. Josowicz, and A. Hierlemann, "CMOS electrochemical DNA-detection array with on-chip ADC," *Proc. ISSCC Dig. Tech. Papers*, pp. 167–168, Feb. 2008.

[15] H. Wang, Y. Chen, A. Hassibi, A. Scherer, and A. Hajimiri, "A frequency-shift CMOS magnetic biosensor array with single-bead sensitivity and no external magnet," *Proc. ISSCC Dig. Tech. Papers*, pp. 438–439, Feb. 2009.

[16] S. Joo and R. B. Brown, "Chemical sensors with integrated electronics," *Chem. Rev.*, vol. 108, pp. 638–651, 2008.

[17] E. Katz and I. Willner, "Probing biomolecular interactions at conductive and semiconductive surfaces by impedance spectroscopy: routes to impedimetric immunosensors, DNA-sensors, and enzyme biosensors," *Electroanalysis*, vol. 15, no. 11, pp. 913–947, Feb. 2003.

[18] J. S. Daniels and N. Pourmand, "Label-free impedance biosensors: opportunities and challenges," *Electroanalysis*, vol. 19, no. 12, pp. 1239–1257, May 2007.

[19] K. Solly, X. Wang, X. Xu, B. Strulovici, and W. Zheng, "Application of real-time cell electronic sensing (RT-CES) technology to cell-based assays," *Assay Drug Dev. Technol.*, vol. 2, pp. 363–372, 2004.

[20] B. Eversmann, M. Jenkner, F. Hofmann, C. Paulus, R. Brederlow, B. Holzapfl, P. Fromherz, M. Merz, M. Brenner, M. Schreiter, R. Gabl, K. Plehnert, M. Steinhauser, G. Eckstein, D. Schmitt-Landsiedel, and R. Thewes, "A $128 \times 128$ CMOS biosensor array for extracellular recording of neural activity," *J. Solid-State Circuits*, vol. 38, no. 12, Dec. 2003.

[21] E. M. Maynard, C. T. Nordhausen, and R. A. Normann, "The Utah intracortical electrode array: A recording structure for potential brain-computer interfaces," *Electroencephal. Clin. Neurophysiol.*, vol. 102, no. 3, pp. 228–239, Mar. 1997.

[22] P. J. Rousche, D. S. Pellinen, D. P. Pivin, J. C. Williams, R. J. Vetter, and D. R. Kipke, "Flexible polyimide-based intracortical electrode arrays with bioactive capability," *IEEE Trans. Biomed. Eng.*, vol. 48, no. 3, Mar. 2001.

[23] M. Mojarradi, D. Binkley, B. Blalock, R. Andersen, N. Ulshoefer, T. Johnson, and L. Del Castilloadi, "A miniaturized neuroprosthesis suitable for implantation into the brain," *IEEE Trans. Neural Syst. Rehab. Eng.*, vol. 11, no. 1, Mar. 2003.

[24] K. Owino and O. A. Sadik, "Impedance spectroscopy: A powerful tool for rapid biomolecular screening and cell culture monitoring," *Electroanalysis*, vol. 17, pp. 2101–2113, 2005.

[25] P. J. Roberts-Thomson and K. Shepherd, "Molecular size heterogeneity of immunoglobulins in health and disease," *Clin Exp. Immunol.*, vol. 79, pp. 328–334, Mar. 1990.

[26] F. Patolsky, E. Katz, A. Bardea, and I. Willner, "Enzyme-linked amplified electrochemical sensing of oligonucleotide-DNA interactions by means of the precipitation of an insoluble product and using impedance spectroscopy," *Langmuir*, vol. 15, pp. 3703–3706, Apr. 1999.

[27] F. Lucarelli, G. Marrazza, A. P. F. Turner, and M. Mascin, "Carbon and gold electrodes as electrochemical transducers for DNA hybridisation sensors," *Biosens. Bioelectron.*, vol. 19, no. 6, pp. 515–530, Jan. 2004.

[28] N. Patel, M. C. Davies, M. Hartshorne, R. J. Heaton, C. J. Roberts, S. J. B. Tendler, and P. M. Williams, "Immobilization of protein molecules onto homogeneous and mixed carboxylate-terminated self-assembled monolayers," *Langmuir*, vol. 13, pp. 6485–6490, 1997.

[29] J. D. Plummer, M. D. Deal, and P. B. Griffin, *Silicon VLSI Technology*. Upper Saddle River, NJ: Prentice-Hall, 2000.

[30] P. H. Gimenez, J. J. Rameau, and M. C. Rebou, "Experimental pH potential diagram of aluminum for sea water," *Corrosion*, vol. 37, no. 12, pp. 673–682, 1981.

[31] *Specification for Electroless Nickel/Immersion Gold (ENIG) Plating for Printed Circuit Board*, IPC Std. 4522.

[32] J. Stettner and A. Winkler, "Characterization of alkanethiol self-assembled monolayers on gold by thermal desorption spectroscopy," *Langmuir*, vol. 26, pp. 9659–9665, 2010.

[33] A. E. Gamal and H. Eltoukhy, "CMOS image sensors," *IEEE Circuits Devices Mag.*, vol. 21, no. 3, May 2005.

[34] T. H. Lee, *The design of CMOS radio-frequency integrated circuits*. Cambridge, U.K.: Cambridge Univ. Press, 1998.

[35] I. M. Filanovsky and H. Baltes, "CMOS schmitt trigger design," *IEEE Trans. Circuits Syst. I, Fndam. Theory Appl.*, vol. 41, no. 1, pp. 46–49, Jan. 1994.

[36] A. Hassibi, H. Vikalo, and A. Hajimiri, "On noise processes and limits of performance in biosensors," *J. Appl. Phys.*, vol. 102, no. 1 (014909), Jul. 2007.

[37] A. J. Bard and L. R. Faulkner, *Electrochemical Methods: Fundamentals and Applications*. New York: Wiley, 2001.

[38] E. Boubour and R. B. Lennox, "Insulating properties of self-assembled monolayers monitored by impedance spectroscopy," *Langmuir*, vol. 16, pp. 4222–4228, 2000.

[39] J. R. Macdonald and J. A. Garber, "Analysis of impedance and admittance data for solids and liquids," *J. Electrochem. Soc.*, vol. 124, no. 7, 1977.

[40] Y. Jung, J. M. Lee, H. Jung, and B. H. Chun, "Self-directed and self-oriented immobilization of antibody by protein G-DNA conjugate," *Anal. Chem.*, vol. 79, pp. 6534–6541, 2007.

[41] K. S. Ma, H. Zhou, J. Zoval, and M. Madou, "DNA hybridization detection by label free versus impedance amplifying label with impedance spectroscopy," *Sens. Actuators B, Chem.*, vol. 114, no. 1, pp. 58–64, Mar. 2006.

[42] B. B. Haab, "Methods and applications of antibody microarrays in cancer research," *Proteomics*, vol. 3, no. 11, p. 2116, 2003.

[43] Y. M. Bae, B. K. Oh, W. Lee, W. H. Lee, and J. W. Choi, "Detection of insulin-antibody binding on a solid surface using imaging ellipsometry," *Biosens. Bioelectron.*, vol. 20, no. 4, pp. 895–902, Nov. 2004.


**Arun Manickam** received the M.Sc. degree from the University of Texas at Austin in 2008, where he is currently pursuing the Ph.D. degree in electrical and computer engineering.

His research interests are integrated-circuit design for biomedical applications and interface modeling. His current research is on developing models for electrodes used in bioelectronic systems and the design of an impedance spectroscopy system-on-a-chip.

**Aaron Chevalier** received the B.A. degree in physics from The University of Texas at Austin in 2007, where he is currently pursuing the M.Sc. degree in biomedical engineering.

His research interests are in biosensor assay development and real-time microarrays.

**Mark McDermott** received the B.S. degree in electrical engineering from the University of New Mexico, Albuquerque, and the M.S. degree in electrical engineering from the University of Texas at Austin.

Currently, he is a Research Fellow in the Electrical and Computer Engineering Department at the University of Texas at Austin where he teaches graduate-level courses in very-large scale integration design, system-on-chip design, and technical entrepreneurship. His current interests include research on methodologies to improve design and verification productivity in silicon system design. Previously he was the Vice-President (VP) of Engineering at Coherent Logix; CEO of DynaFlow Computing, Inc.; VP of Engineering and Co-Founder of Somerset Embedded Technologies, Inc.; VP of Engineering and Co-Founder of VisionFlow, Inc.; General Manager of the Texas Development Center for Intel Corporation; Director of the PowerPC Somerset Design Center; and Director of the Austin Design Center for Cyrix, Inc.

Mr. McDermott is a registered professional engineer and a member of the IEEE, ACM and TSPE. He has 19 patents and a number of publications in the areas of IC design and engineering management. He is on the technical advisory boards of Obsidian Software Inc., Nascentric, Inc., Innovative Silicon, Inc. and Pyxis, Inc.

**Andrew D. Ellington** received the B.S. degree in biochemistry from Michigan State University, Ann Arbor, in 1981, and the Ph.D. degree in biochemistry and molecular biology from Harvard University, Cambridge, MA, in 1988.

As a graduate student, he worked with Dr. Steve Benner on the evolutionary optimization of dehydrogenase isozymes. His postdoctoral work was with Dr. Jack Szostak at Massachusetts General Hospital, where he developed methods for the *in vitro* selection of functional nucleic acids and coined the term "aptamer." He began his academic career as an Assistant Professor of Chemistry at Indiana University in 1992, and continued to develop selection methods.

Dr. Ellington received the Office of Naval Research Young Investigator, Cottrell, and Pew Scholar awards. In 1998, he moved to the University of Texas at Austin and is currently the Fraser Professor of Biochemistry. His lab now works on the development of functional nucleic acids for practical applications, including aptamer biosensors, allosteric ribozyme logic gates (aptazymes), and internalizing nucleic acids that can deliver siRNAs to cells. His next accomplishment is to hopefully develop synthetic genetic circuits that can perform amorphous computations.

**Arjang Hassibi** received the B.Sc. degree (Hons.) in electrical engineering from the University of Tehran, Tehran, Iran, in 1997, and the M.S. and Ph.D. degrees in electrical engineering from Stanford University, Stanford, CA, in 2001 and 2005, respectively.

From 2005 to 2006, he was a Postdoctoral Scholar in the Department of Electrical Engineering at the California Institute of Technology. Since 2006, he has been with the Department of Electrical and Computer Engineering of the University of Texas at Austin where he is currently an Assistant Professor. He has also held research positions at IBM T.J. Watson Reserach Center, Barcelona Design, Stanford Genome Technology Center, and Xagros Genomics, which he co-founded in 2001. His areas of interest are complementary metal–oxide semiconductor biochips, analog and mixed-signal circuit design, biotechnology, and spectroscopy.